Journal of Energy Storage 73 (2023) 108811

Contents lists available at ScienceDirect

Journal of Energy Storage

journal homepage: www.elsevier.com/locate/est

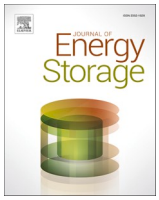

Research Papers

Chemical synthesis of polyaniline and polythiophene electrodes with excellent performance in supercapacitors

Anjana Ramesh Peringath [a,1], Mohammad A.H. Bayan [b,1], Mustehsan Beg [c], Amrita Jain [b], Filippo Pierini [b], Nikolaj Gadegaard [a], Richard Hogg [a], Libu Manjakkal [a,c,*]

[a] James Watt School of Engineering, University of Glasgow, Glasgow G12 8LT, UK
[b] Institute of Fundamental Technological Research, Polish Academy of Sciences, Pawińskiego 5B, 02-106 Warsaw, Poland.
[c] School of Computing and Engineering & the Built Environment, Edinburgh Napier University, Merchiston Campus, EH10 5DT, UK.

ARTICLE INFO

Keywords:
Conductive polymers
Spin coating
Polyaniline
Polythiophene
Supercapacitor
Electrochemical performances

ABSTRACT

The emergence of portable electronics in miniaturized and intelligent devices demands high-performance supercapacitors (SC) and batteries as power sources. For the fabrication of such energy storage devices, conducting polymers (CPs) have significant advantages due to their high theoretical capacitive performance and conductivity. In this work, we developed two CPs including polyaniline and polythiophene through a low-cost chemically synthesized approach and the film-by-spin coating method. The structural and morphological properties of the CPs are analyzed using Fourier-transform infrared spectroscopy (FTIR), contact angle measurement, and scanning electron microscopy (SEM). Based on these CPs, novel pristine polyaniline and polythiophene-based SCs (PASC and PTSC) are developed. The prepared CPs contribute to high electrochemical performances due to their high conductive nature of the electrode and conjugated polymer materials reaction. Hence both electrochemical double-layer formation and pseudocapacitance contributed to the energy-storing performances of the device. Electrochemical impedance spectroscopic analysis (0.1 Hz to 100 kHz) demonstrates faster ionic exchange and high capacitance of the PASC electrode as compared to PTSC in H_3PO_4 electrolyte. The PASC devices exhibit specific capacitance of 13.22 $mF{\cdot}cm^{-2}$ with energy and power densities of 1.175 $\mu W{\cdot}h{\cdot}cm^{-2}$ and 4.99 $\mu W{\cdot}cm^{-2}$ at a current of 50 μA. Compared to PTSC (specific capacitance 3.30 $mF{\cdot}cm^{-2}$) the PASC shows four times higher specific capacitance due to its improved surface, structural and electrical properties. The electrochemical performance reveals the superior SC performance for this type of CP electrode.

1. Introduction

Smart energy storage devices such as batteries and supercapacitors (SC) with long life cycles exhibit potential advantages in low-powered electronics, especially for portable devices [1–4]. For future use in the future generation of energy storage devices, SCs exhibit significant advantages including extended lifecycle, fast charging and discharging, high power density, efficient charge storage process, and high energy density [5–9]. Furthermore, SCs have seen widespread usage in various industries including transportation, electronics, military, aerospace, and sensors, among others [8,10–12]. Most of the research in SCs has been focused on the synthesis of new materials and the design of new devices. For this purpose, various carbon structures, metal oxides, polymers, and composite materials have been used [13–15]. To deliver sustainable new SCs, it is necessary to perform materials/device synthesis from non-toxic, low-cost materials. Among various choices, conducting polymers (CPs) are characterised by their environmental friendliness, ease of processing, low cost, adjustable conductivity via doping, and high capacitance which makes them an ideal candidate for the electrode material for SCs [16–18].

Over the past few years, several CPs have been developed and utilised in various fields such as polymer light-emitting diodes [19,20], sensors [21–23], artificial muscles [24–26], anti-corrosion coating [27,28], and energy storage devices [16–18,29]. The high pseudocapacitance due to the conjugated materials, accessible redox states for electrolyte reaction, and controllable physical properties lead CPs to be

* Corresponding author at: School of Computing and Engineering & the Built Environment, Edinburgh Napier University, Merchiston Campus, EH10 5DT, UK.
E-mail address: L.Manjakkal@napier.ac.uk (L. Manjakkal).
[1] Equal authors.

https://doi.org/10.1016/j.est.2023.108811
Received 17 April 2023; Received in revised form 10 July 2023; Accepted 22 August 2023
Available online 30 August 2023

an excellent energy-storing material [29,30]. CPs backbone is a highly delocalised π-electron system with alternating single and double bonds [30]. Furthermore, the π-conjugation results in molecular orbitals with high energy occupancy and low energy unoccupancy, creating a readily oxidisable or reducible system [31]. Moreover, unlike traditional insulating polymers, CPs are semiconducting and can be doped to exhibit metallic conductivity [31,32]. The high conductivity and redox active sites lead to the combined effects of electrochemical double layer capacitance (*EDLC*) and pseudocapacitance formation in CP based SCs. For energy storage device fabrication the most extensively researched CPs are polypyrrole (PPy) [33,34], polyaniline (PANI) [35], poly(3,4-ethylenedioxythiophene)-poly(styrenesulfonate) (PEDOT:PSS) [16,29], polythiophene (PTh) [36,37] and their derivatives or composites [38,39]. It has been found that various methods and different designs may be employed for CPs based SC fabrications. To enhance the performances of CP-based SCs, the majority of work has reported the development of composite film or layered electrodes with different materials including metal oxide or MXene [40,41]. Such devices exhibited high specific capacitance, for example MXene/CNF/PANI electrode boasts a high areal specific capacitance of 2935 $mF{\cdot}cm^{-2}$ at a current density of 1 mA cm^{-1} [42]. From the different methods of SC development, solution-processed methods are highly advantages for CP based SCs due to the possibility of large-scale production, ease of fabrication of electrodes, and low cost. The SC performance of several CP based SCs are summarized in Table S1 in supporting information. It was observed that spin coating is very convenient for the development of small area SCs for low powered electronics.

In this paper we describe the development of new PANI and PTh based SCs (PASC and PTSC, respectively) and investigate their electrochemical performances. Compared to the reported PANI and PTh based SCs (as shown in Table S1), in this work we utilize pristine polymers without any composite formation. For the development of SC electrodes, the PANI and PTh were synthesized in a simple and low-cost method. The electrode materials were synthesized by using a three-neck flask with a magnetic stirrer, and a nitrogen inlet, positioned in a water-ice bath. The prepared CP solution was spin coated as an active electrode of the SC on the top of a graphite current collector. The prepared conductive electrodes showed excellent electrical and electrochemical stability, described herein. PANI has a distinctive method of conductivity and remarkable electrochemical performance, with a high theoretical specific capacitance making it an exceptional pseudocapacitive material [43]. PTh is well-suited for SC fabrication due to its exceptional pseudocapacitance, strong electrical conductivity, high energy density, low cost, and environmentally friendly properties [44]. For evaluation of the electrode performance in this study, we used two different electrolytes such as KCl and H_3PO_4, with a polyester/cellulose separator. Through electrochemical studies such as cyclic voltammetry (CV), electrochemical impedance spectroscopy (EIS) and galvanostatic charging discharging (GCD) we found that the PASC in H_3PO_4 shows better performances due to the excellent property of PANI electrode. The fabricated PASC shows comparatively better or similar performance with other reported CPs based SCs as summarized in Table S1.

2. Experimental section

2.1. Materials

Double-distilled aniline (99.5 %) and thiophene (99.0 %), ammonium peroxydisulfate (APS, 98 %), triethanolamine (TEA, 99 %), sodium dodecyl sulfate (SDS), hydrochloric acid (HCl, 37 %), *N*,*N*-dimethylformamide (DMF, 99.8 %), hexafluoro-2-propanol (HFIP, 99 %), and methanol (99.9 %) were all purchased from Sigma Aldrich Company. Graphite sheets were purchased from SGL Carbon (0.5 mm, Germany).

2.2. Synthesis of polyaniline and polythiophene

To synthesize emeraldine PANI, a three-neck flask with a magnetic stirrer was used. The reactor flask was equipped with a nitrogen inlet and a droplet injection system. The flask was placed in a water-ice bath. Before pouring the materials into the reactor and starting the synthesis, the input nitrogen pressure of the reactor was controlled, and the bath temperature was set at 0 °C; the rotation rate was at 450 rpm. The duration of semi-continuous feeding was adjusted to approximately 25 min. In the next step, aniline (300.0 μl) was gradually added to 30.0 ml of 1.0 M aqueous solution of HCl. When aniline dissolved in HCl solution, it was moved to the reaction flask to reach the synthesis temperature. Afterward, the initiator APS (303.0 μl) was dissolved in 30.0 ml of 1.0 M HCl solution and then transferred to the droplet injection system. When the first drops of initiator enter the reaction container, the polymerization starts. While the reaction is progressing, the reaction mixture after 3 h gradually turns emerald green and becomes completely uniform. At the end of the reaction after 24 h, a small amount of methanol (100 μl) was added to the balloon. The magnetic stirrer was stirred until the containing solution of synthesized polymer was separated and precipitated. Then the reactor was evacuated, and the harvested polymer solution was passed through a filter paper. After three methanol washes and two distilled water washes it became smooth. At that point, the filter containing the polymer was placed in a vacuum oven for 6 h at 50 °C. After this stage, the weight of the filter remains stable. The scheme of the PANI synthesis and film fabrication procedure can be found in Fig. 1a.

The procedure of synthesis of PTh was conducted in the same reaction flask as PANI. Initially, 2.5 ml of thiophene, 1.0 g SDS, and 9.5 ml of TEA were mixed with 30.0 ml of DI water in a reaction container and magnetically stirred to prepare a homogenous solution of monomer. Concurrently, APS was dissolved in 20.0 ml of DI water and was transferred into the feeding injection system. The molar ratio of the initiator to monomer was 1.15. After filling the flask with a nitrogen inlet, the initiator was introduced. The early stage of polymerization was confirmed by the color change of the solution. The polymerization was allowed to proceed for 24 h. Subsequently, the final dark brown precipitate was collected by centrifugation. To separate the oligomers and impurities from the desirable product, the polymerization product was washed three times with DI water and methanol and finally freeze-dried. The steps of preparation given of PTh are given in Fig. 1b.

2.3. Fabrication of polymer thin film

The graphite substrate was cleaned by rinsing several times with distilled water and methanol in an ultrasonic bath and dried under a nitrogen flow. Then a PANI layer was spin-coated on graphite at 1000 rpm for 60 s and subsequently annealed at 70 °C for 5 min. The PANI precursor solution was prepared by filtering with a PTFE syringe filter (Whatman, 0.45 mm) and dissolving in HFIP at 10 % w/w. To prepare a thin film of PTh, the freshly synthesized polymer first dissolves in DMF with a ratio of 5 % w/w. Subsequently, the polymer solution was spin-coated on the clean graphite sheet at 1000 rpm and for 60 s and annealed at 65 °C for 5 min.

2.4. Fabrication of supercapacitors

In the previous stage, the active electrodes were applied on the top surface of the graphite sheet. For the underside of the graphite, the wires were attached for measurement purposes using silver paste (RS components). The wires were securely attached at a temperature of 80 °C for 30 min in an oven and subsequently covered with an insulating ink (JE solution). The insulating ink was then subjected to a curing process at 80 °C for 1 h in an oven. In this work, two symmetric SCs were fabricated using PANI and PTh as the active materials, termed PASC and PTSC, respectively. For the fabrication of the SCs, the electrodes were used

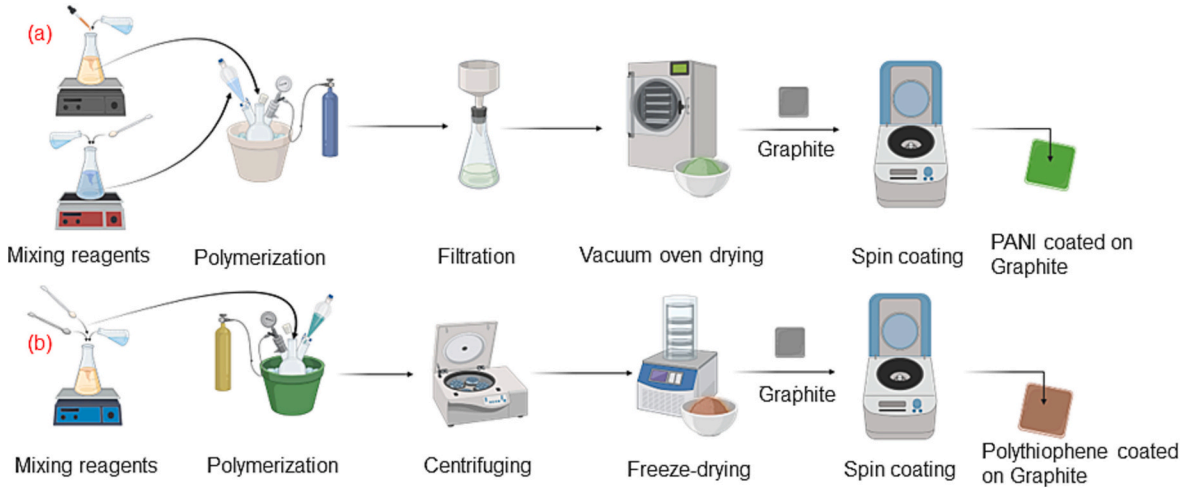

Fig. 1. Schematic representation of synthesis and film fabrication on graphite current collector of (a) PANI and (b) PTh.

with a polyester separator (Techni Cloth (TX 612), which was soaked in H_3PO_4 electrolyte. We also compared the performances of the electrodes in a 1 M KCl electrolyte. The schematic of the device is given in Fig. 2a and b shows the electrode reaction with the electrolyte.

2.5. Characterisation

To investigate the physio-chemical characterizations of the synthesized polymers, Fourier-transform infrared spectroscopy (FTIR, Perkin Elmer ATR 100 instrument, USA) analysis was performed. UV–Vis spectra detection of conjugated polymers was measured using a spectrophotometer (Multiscan GO Thermo Scientific, USA). The morphology of the polymer film was analyzed using scanning electron microscopy (SEM, JEOL JSM-6390LV) with a 7 kV acceleration voltage and a 10 mm working distance. Prior to the observation, the analyzed polymer samples were coated with a thin layer of gold using a sputter-coating technique. Nitrogen sorption experiments were carried out by using AutoSorb iQ (Quantachrome) system operated at 77 K. The Brunauer–Emmett–Teller (BET) method based on the adsorption data was used to calculate the specific surface area. The total pore volume was obtained from the adsorbed amount of N_2 at P/P0 = 0.99. DFT analysis was used on the adsorption branch to evaluate the average pore diameter. Thermal analysis of pre-heated samples was performed by using TG/DSC analyzer SDT 650, TA Instruments Instrument from room temperature to 850 °C at a heating rate of 5 °C/min under nitrogen atmosphere. Hydrophobicity and hydrophilic nature of the film investigated through contact angle measurement (Contact Angle Goniometer, Oscilla). Electrochemical performances including EIS (100 kHz to 0.1 Hz at 10 mV) and CV (scan rate-10–500 mV s^{-1}) analysis was carried out using electrochemical workstation (Gamry) with H_3PO_4 and KCl electrolyte. The galvanostatic charging discharging (GCD) measurements of the PASC PTSC were tested by using source meter with LabVIEW program (Agilent, U2722A).

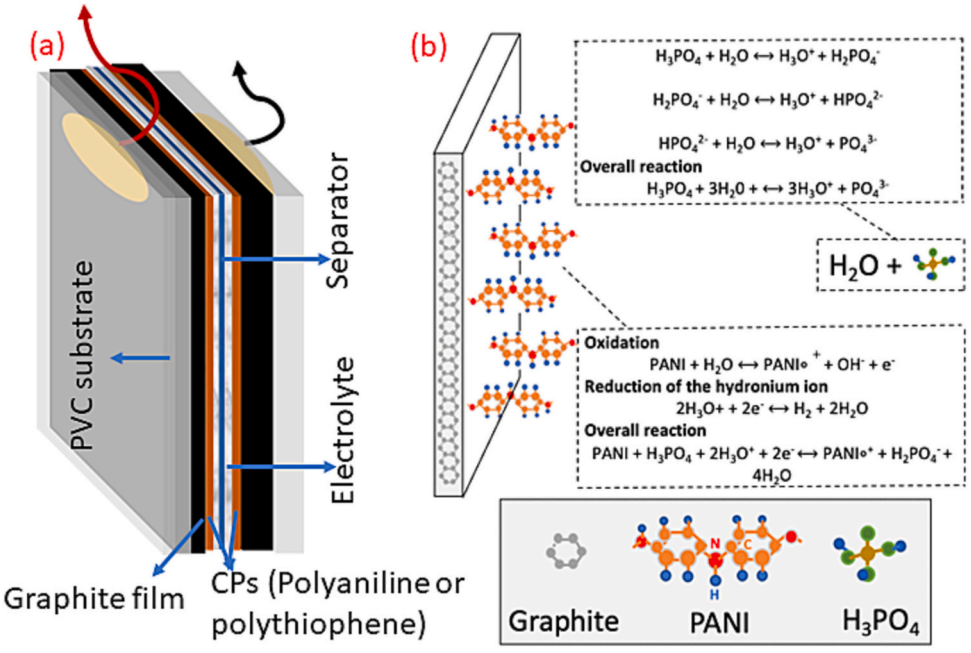

Fig. 2. (a) Schematic representation of developed supercapacitor. (b) Electrode-electrolyte reaction of PANI with H_3PO_4 electrolyte.

3. Results and discussion

3.1. Structural and morphological analysis of the electrodes

Fig. 3a presents the FTIR spectrum of PANI and PTh from 3500 to 500 cm^{-1}. Aniline, as the monomer of PANI, shows a strong peak at 1146 cm^{-1} related to the quinone nitrogen's vibrational modes. Similarly, the peaks at 1439 and 1570 cm^{-1} are related to stretching modes in benzoid and quinoid of benzene in aniline structure. The peak observed at 818 cm^{-1} is related to the configuration change of the C—H bond in benzene. Along with the spectrum of PANI peaks in the range of 2936 and 3433 cm^{-1}, they can be attributed to symmetric and asymmetric configurations of stretching NH^{+}. The transmittance peak in the PANI spectrum confirms the synthesis of emeraldine PANI. The FTIR transmission spectrum of the thiophene exhibited characteristic vibration at 2916 cm^{-1} for C—H stretching vibration bands. The bands at 1674 and 1404 cm^{-1} correspond to C═C asymmetric and symmetric stretching vibrations of the thiophene ring, respectively. The vibration bands observed at 1211 cm^{-1} and 1041 cm^{-1} are due to C—H bending and in-plane deformation. Furthermore, the characteristic bands of PTh are seen at 763 cm^{-1} (C—S bending) and 694 cm^{-1} (C—S—C ring deformation stretching). Results of the FTIR studies clearly indicate the polymerization of the monomer, as illustrated in Fig. 3a.

The UV spectra of PANI and PTh are given in Fig. 3b. The PANI spectrum was measured in MeCN. The UV spectra show a sharp absorption peak at 365 nm. The bipolaron/polaron resonance absorption of the electrons is attributed to the band between 330 and 450 nm. This shows that the conductive emeraldine PANI form was formed using the previously described process. The intensity of this peak indicates that the synthesized polymer is electrically conductive. We also measured the UV–Vis absorbance of PTh in DMF to rule out the possibility that the polythiophene breaks down after polymerization. The UV–Vis spectrum of PTh is shown in Fig. 3b. The expansion of π-conjugation is indicated by the peaks at 446 nm, which are associated with the (π-π*) band of the polymerized monomer. It is important to note that the (π-π*) band's intensity demonstrates that thiophene units do not disintegrate after polymerization.

The surface morphology of coated layers of conjugated polymers were investigated through the SEM micrographs shown in Fig. 4. Fig. 4a to c shows the SEM images of the graphite sheet at different magnifications. The magnified image of the graphite sheet shows the large layer of flake-type structure. The thickness of the graphite sheet used for these samples was approximately 810 μm. On the top of this graphite sheet PTh and PANI were coated. SEM images revealed that the polymer-coated films have two distinct morphologies: porous structure for PTh and non-porous for PANI spin-coated layer. Fig. 4d to f shows SEM images of PTh. It was found that the evaporation of the solvent in which PTh was dissolved led to the creation of a porous network of PTh and is clearly observed in the magnified image in Fig. 4f. The average pores diameter is 159.04 μm ± 61.89 μm for PTh film. By scratching some parts of coated layer prior to SEM, this morphology is more visible and is shown in Fig. 4d (described as not covered for substrate and covered for film coating). However, the PANI coating exhibits a uniform and thin layer of polymer over the graphite sheets' surface (Fig. 4g to i). The spin-coated PANI layer has a flat film without exhibiting any pores on the surface, with an average thickness of 401 nm.

Fig. 5a and Fig. S1a in supporting information shows the N_2 adsorption-desorption studies of PANI and PTh materials. The pore size distribution curves of the PANI and PTh materials are given in Fig. S1b and S1c. As can be seen from the isotherms, that nitrogen adsorption-desorption curve of PANI follows type II isotherm as per IUPAC nomenclature, the flatter region in the middle region represents the formation of monolayer. In the present situation, at low pressure, the micropores were filled with gas, monolayer formation takes place at the middle region and at high pressure, capillary condensation takes place. DFT method was used to calculate the average pore size and micropore volumes. The sample contains the mixture of micropores, mesopores and macropores which confirms the suitability of material for SC application. The specific surface area observed for PANI is 18.01 $m^2\ g^{-1}$ and for PTh is 7.32 $m^2\ g^{-1}$. The results obtained are summarized in Table S2. Fig. 5b shows the thermogravimetric curves of PANI and PTh. It can be seen from the thermal curves that both polymers are thermally stable. The first slight weight loss can be seen at 150 °C which is due to the loss of water content and other solvents. In particular, PANI was stable up to 400 °C and later it decomposes sharply and in case of PTh also, the sample was stable up to 465 °C and later it decomposes but it still the decomposition rate was slow as compared to PANI. From room temperature to 850 °C the total weight loss of PTh was 3.8 % which is in agreement with previous published results, PTh is thermally stable up to 900 °C in inert atmosphere [45]. TGA studies confirm that both the materials were thermally stable and can be used for device application.

Contact angle measurements were carried out to analyze surface wettability of the electrode. It has been found that the surface wettability strongly influences charge accumulation and energy storing performance [46]. Contact-angle measurements reveal that on the top of the PANI the drop is almost fully distributed, however the PTh film is more hydrophobic (θ = 92°) as presented in Fig. S2 in supporting information. The lower hydrophobicity of PANI is due to the surface

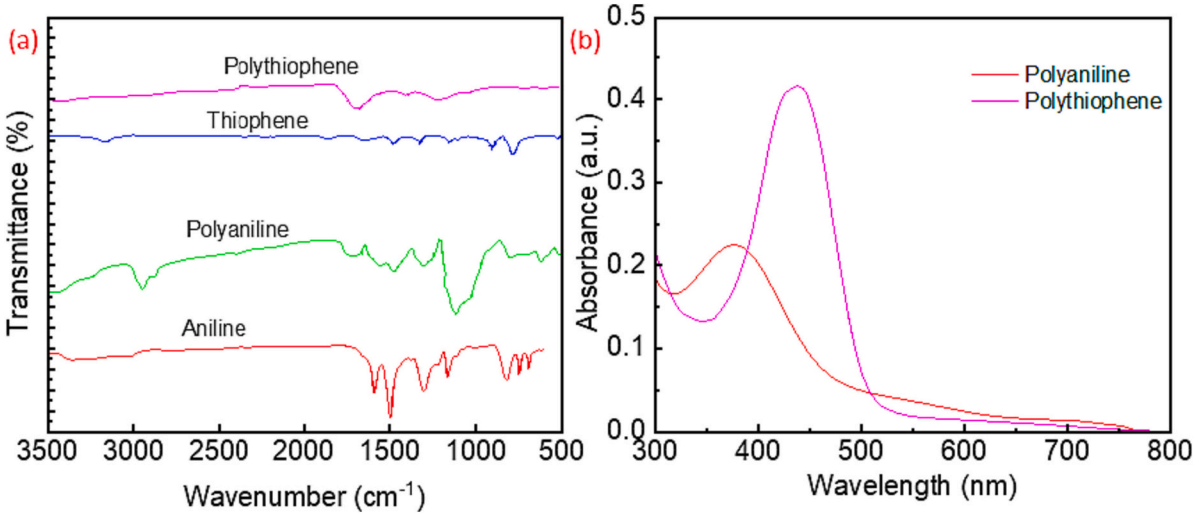

Fig. 3. (a) FTIR spectra and (b) UV–Vis spectra of PANI and PTh films.

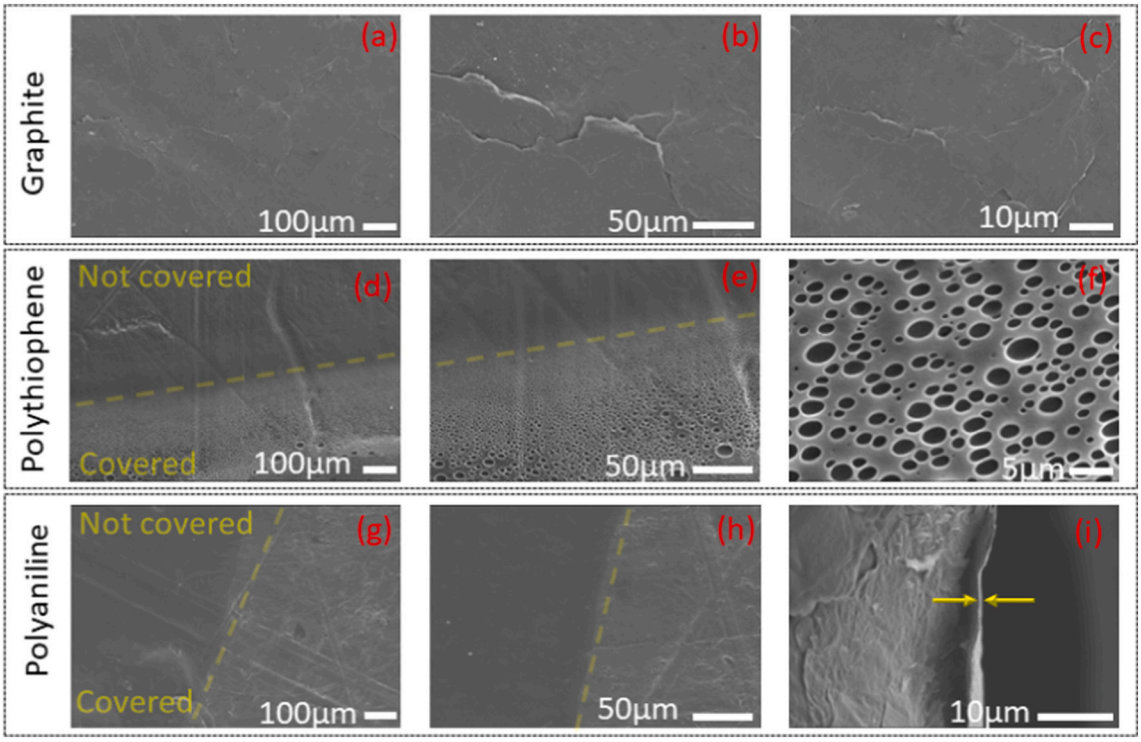

Fig. 4. SEM images of (a–c) graphite sheet and (d–f) PTh film. (g-i) PANI film in different magnifications.

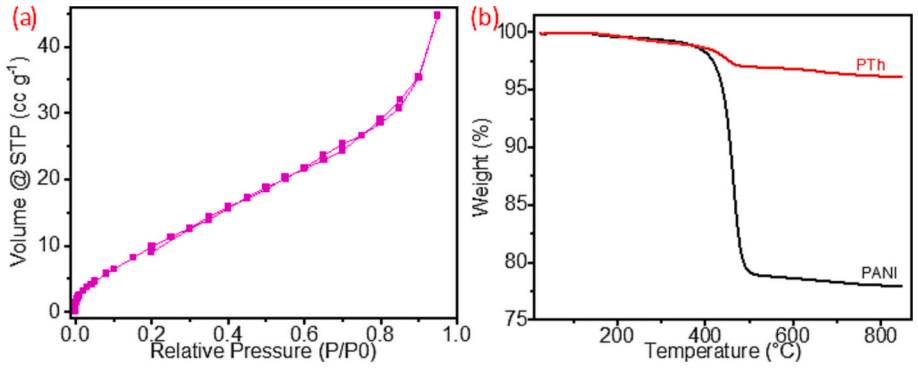

Fig. 5. (a) N_2 adsorption-desorption isotherms of PANI and (b) TGA curves for PANI and PTh.

morphology and leads to better electrode -electrolyte interaction.

3.2. Electrochemical performances of the symmetric SCs

EIS analysis for PASC and PTSC devices were carried out and is presented in Fig. 6. The EIS analysis reveals the ion diffusion and charge transport of the electrodes of the SCs. The Bode impedance and phase angle plots for the frequency range of 100 kHz to 0.1 Hz are shown in Fig. 6a and b. The magnitude of impedance in the Bode plot shows that PASC has a lower impedance as compared to PTSC in both H_3PO_4 and KCl electrolytes. This low impedance value of PASC in H_3PO_4 (Fig. 6a), will lead to faster ionic exchange and high capacitance of the electrode compared with other electrodes. For a frequency of 0.1 Hz the PASC has a capacitance 10.2 mF which is more than four times higher than that of the PASC device with KCl and the PTSC device with H_3PO_4. The variation of capacitance of the PASC and PTSC devices with frequency is given in Fig. S3 in supporting information. The high capacitive nature of PASC supports the results of the Bode phase angle plot in Fig. 6b. As compared to a −90° ideal capacitor phase angle, a value of almost −60° is observed for PASC in H_3PO_4 and KCl electrolytes and is lower for PTSCs (see Fig. 6b). This variation in phase angle could be due to the high capacitance of PASCs and high ionic permeability.

Nyquist plots in Fig. 6c to f show that both PASC and PTSC devices demonstrate diffusion-controlled Warburg capacitive behavior. A near straight line is observed from the Nyquist plot at the lower frequency region, confirming such capacitive behavior [29]. This lower impedance is due to the diffusion of ions from the electrolyte towards the electrode surface. PTSC exhibits higher resistance as compared to PASC which is seen in Fig. 6d in H_3PO_4 electrolyte and in 6f in KCl electrolyte, leading to lower capacitance. The equivalent series resistance (ESR) is determined from the high frequency (here measured at 10 kHz) intercept of Z_{real} in the Nyquist plot. The ESR values measured from Fig. 6c to f and is found that 0.86 Ω for PASC in H_3PO_4, 8.3 Ω for PTSC in H_3PO_4 electrolyte. It was observed that, the PASC with H_3PO_4 electrolyte shows the lowest value of ESR and highest value 18.83 Ω observed for PTSC with KCl electrolyte. The absence of a semi-circle shape in the high frequency range in the Nyquist plots implies better pore accessibility for the electrolyte ions during electrochemical reaction without any charge transfer resistance.

CV analysis of the PASC and PTSC devices was carried out under

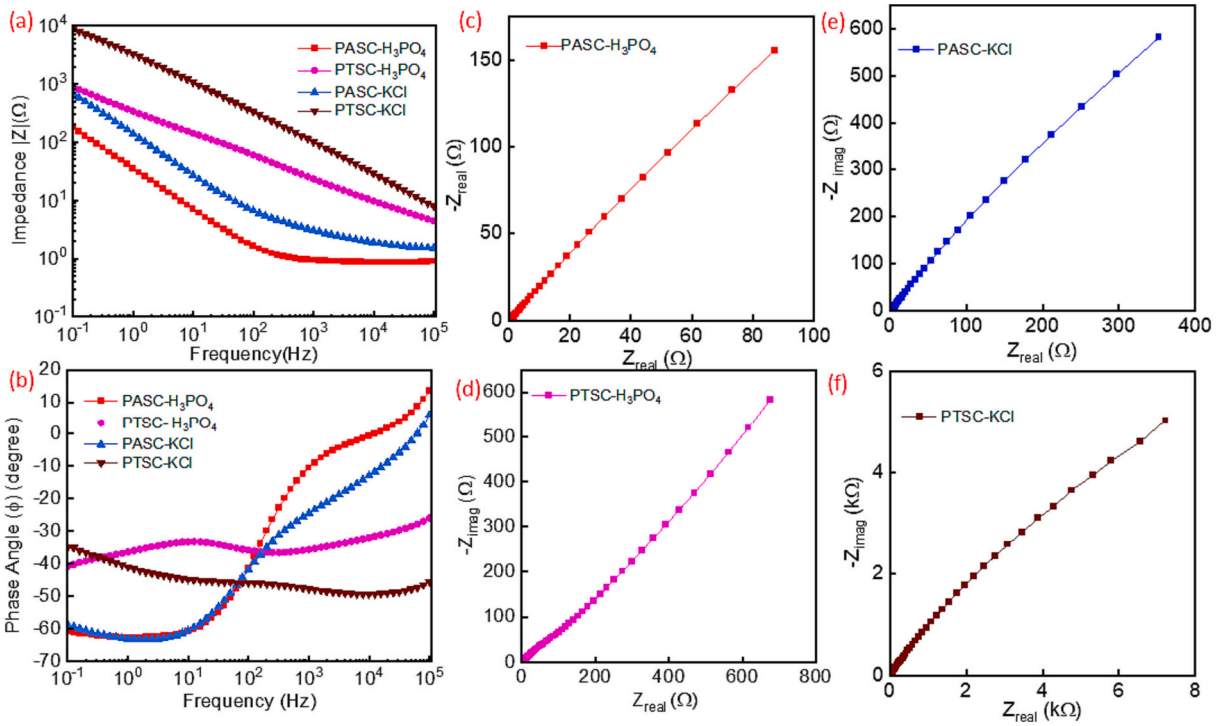

Fig. 6. EIS analysis of PASC and PTSC (a) and (b) Bode impedance plot for PASC and PTSC in H_3PO_4 and KCl electrolytes. (c)–(f) show the Nyquist plot for PASC and PTSC.

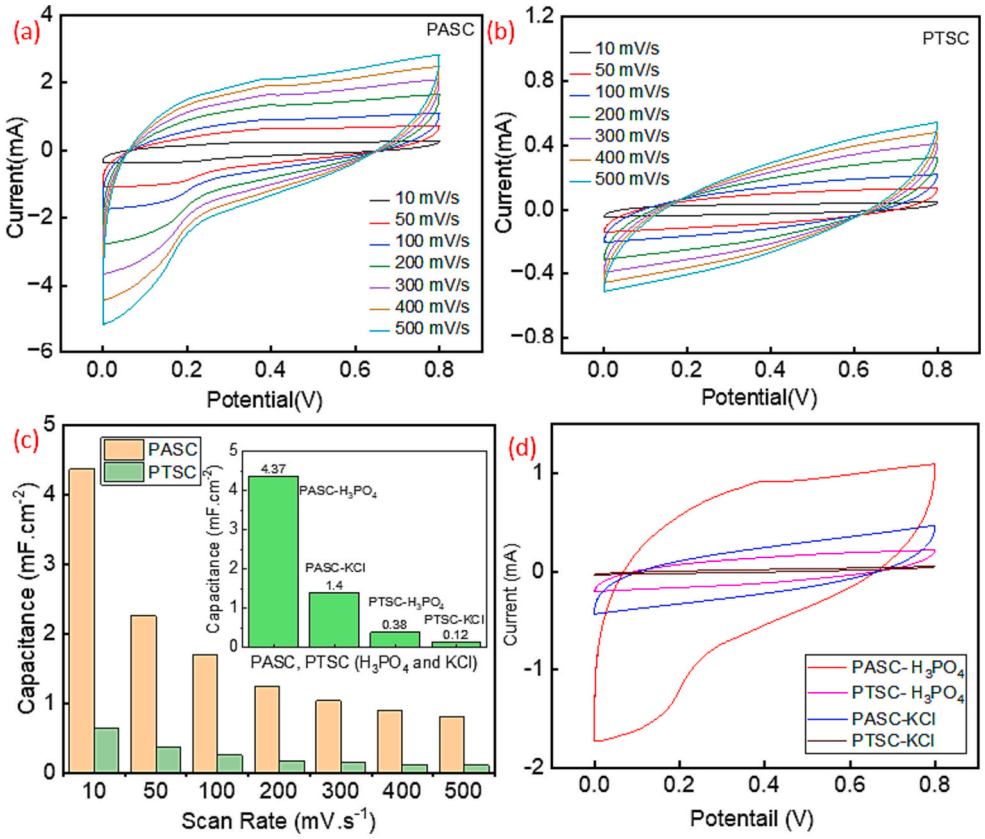

Fig. 7. (a) and (b) CV curves of PASC and PTSC at a scanning rate range of 10-500 $mV{\cdot}s^{-1}$, (c) capacitance of PASC and PTSC in H_3PO_4 electrolyte at different scan rate and the inset shows the capacitance variation for both electrolyte (d) comparison of CV curves for PASC and PTSC in H_3PO_4 and KCl electrolyte at 100 $mV{\cdot}s^{-1}$.

different scan rates in the range of 10–500 mV·s^{-1} for an operating potential window of 0–0.8 V. Fig. 7a and b shows CV curves for PASC and PTSC with H_3PO_4 electrolyte. A similar comparison was carried out for KCl electrolyte and is shown in Fig. S4 in supporting information. From Fig. 7a and b, it is observed that the CV curves maintain a nearly uniform shape at both low and high sweep rates, indicating that the material has an excellent rate stability. The CV curve demonstrates an increase in current with increasing scan rate, indicating an increase in charge accumulation on the electrodes at higher rates and the domination of diffusion reactions [29,47]. Fig. 7a and b shows that both PASC and PTSC have different shapes of their CV curves. The quasi rectangle with peaks shows the electrochemical redox reaction of PASC and PTSC due to the presence of pseudocapacitance of the conducting polymer. The capacitance value 4.37 mF·cm^{-2} for PASC and 0.38 mF·cm^{-2} for PTSC were calculated from the CV at 10 mV·s^{-1} and confirms that PASC devices show more than 10 times higher energy storing performance compared to PTSC. The variation of capacitance with scan rate for PASC and PTSC given in Fig. 7c. From the analysis, it was found that as compared to PTh based electrodes, PANI devices store more charge and have high capacitance due to the combined effect of better electrode-electrolyte interaction (as shown in EIS analysis) and higher specific capacity. This could be found in the larger area of the CV curve at 100 mV·s^{-1} as shown in Fig. 7d. Furthermore, for both PASC and PTSC it was found that the acquired current increased with the scan rate, confirming the diffusion of ions. Additionally, when comparing the performance of both SCs, the SC in H_3PO_4 electrolyte shows high energy storage performance as compared to KCl electrolyte, as shown in Fig. 7c.

Further verification of the electrochemical performance of PASC and PTSC device was obtained by GCD measurement. During the experiment, the voltage of constant charge and discharge was 0.8 V, and the current was 50 μA. From Fig. 8, it can be seen that the curve has a negligible voltage drop during the discharge indicating that the internal resistance of the electrode material is negligible. At the same time the curve still maintains a symmetrical triangular shape. Indicating that the electrode material has excellent electrochemical reversibility. The GCD measurements of the fabricated PASC in H_3PO_4 electrolyte is shown in Fig. 8a and it reveals that PANI possesses the largest capacitance of 13.22 mF·cm^{-2}. The power density of PASC was calculated to be 4.99 μW cm^{-2}, while its energy density was determined to be 1.175 μW·h·cm^{-2}. From Fig. 7b the PTSC shows capacitance of 3.301 mF·cm^{-2} with energy density of 0.29 μW·h·cm^{-2}. In addition to this, we also measured the specific capacitance of PASC and PTSC in KCl, which is shown in Fig. 8c and d and is found to be 7.87 mF·cm^{-2} and 0.77 mF·cm^{-2} respectively. The coulombic efficiency (CE) of the SCs was measured from the GCD analysis and is found 89.7 % for PASC in H_3PO_4, 85.37 % for PTSC in H_3PO_4, 70.6 % for PASC in KCl and 50.7 % for PTSC in KCl electrolyte. It was noticed that depending on types of the conducting polymers and the electrolyte the CE value is changing. It could be due to the resistance variation of the electrode while reacting with electrolyte and is noticed in EIS analysis. Further for the conducting polymer films are found to expand and contract during electrochemical oxidation and reduction. These structural changes can hinder the movement of ions and electrons, resulting in reduced CE [48]. The graph The GCD analysis also predicts that the PASC in H_3PO_4 electrolyte shows better performance, and its values are comparable or better than with other solution based PASC [49,50], as described in Table S1 in supporting information.

We observed PASC in H_3PO_4 electrolyte shows better electrochemical performance and were then tested for multiple charging/discharging cycles. We carried out GCD analysis for 11,000 cycles and

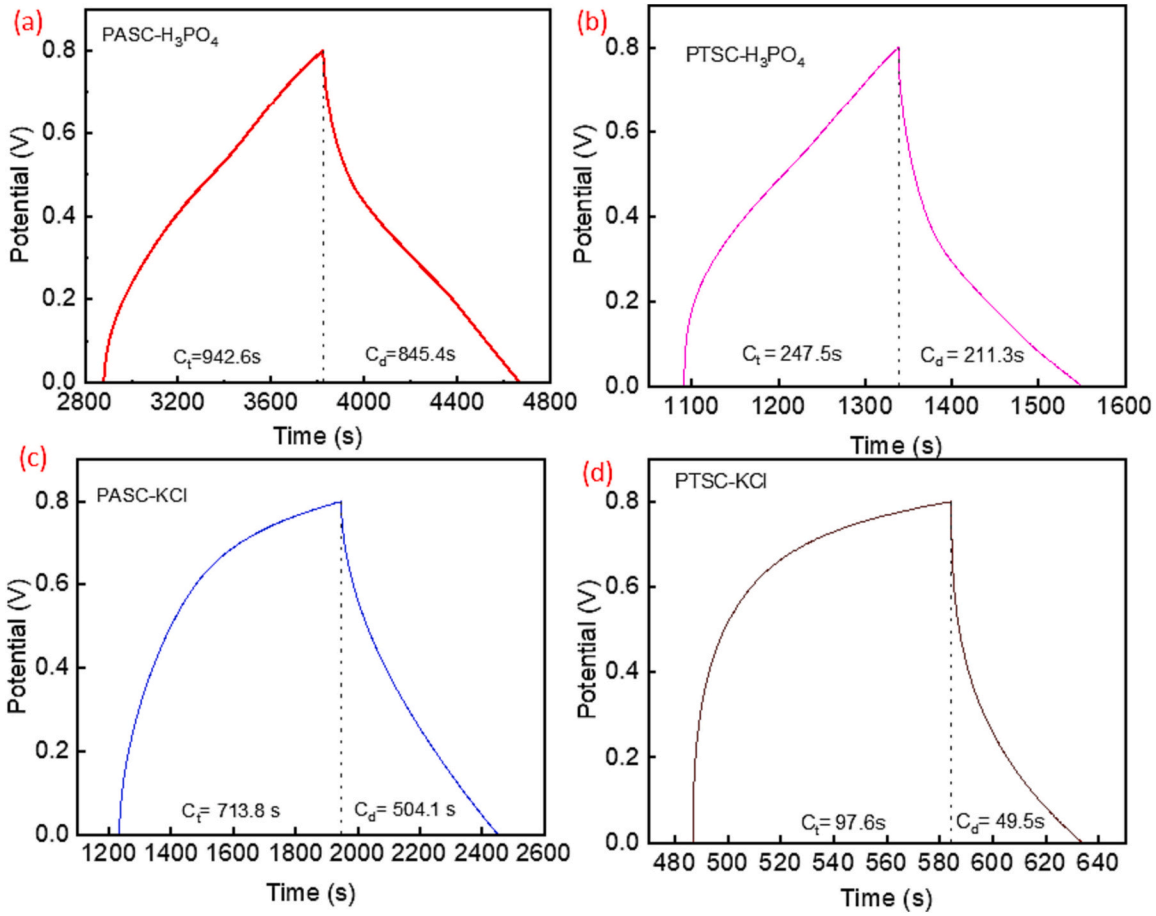

Fig. 8. The GCD analysis of (a) PASC in H_3PO_4 (b) PTSC in H_3PO_4 (c) PASC in KCl and (d) PTSC in KCl electrolyte at applied current density of 12.5 μA·cm^{-2}.

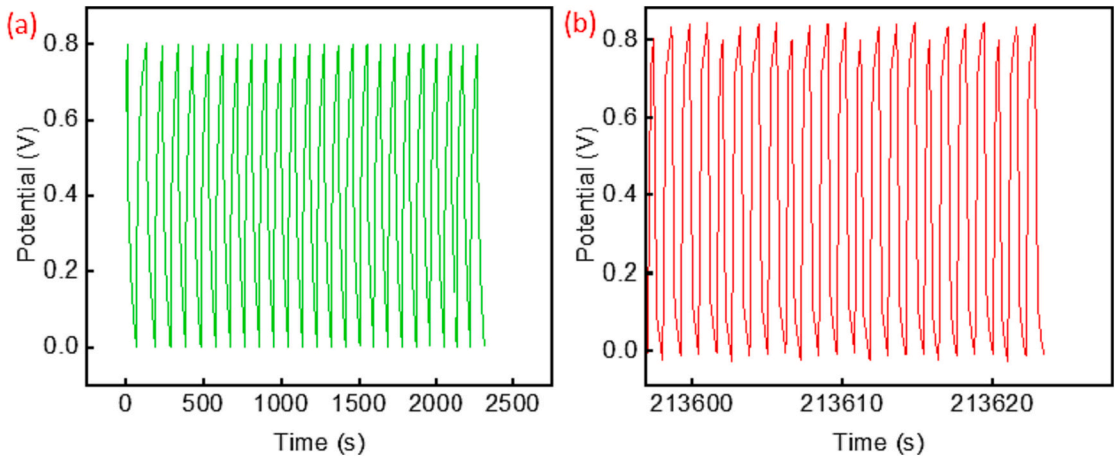

Fig. 9. Long charging discharging cyclic measurement of the PASC (a) for first few cycles and (b) last few cycles of 11,000 cycle measurement.

Fig. 9a shows the cycle performances for the first few cycles, and the final cycles are shown in Fig. 9b. As compared to the first few cycles, we note rapid charging/discharging for last few cycles, as shown in Fig. S5 in supporting information. The device exhibited 62 % of capacitive retention after 1000 cycles. In future, these SCs could be integrated in power management circuits for operating low powered sensors and electronic components for wearables and smart devices [5,51,52]. To improve the CE, and the performances for advanced applications, a composite of PANI and PTh with other materials including metal oxide and reduced graphene oxide will be prepared [53,54].

4. Conclusion

In this work two symmetric SCs were developed using polyaniline and polythiophene based conductive polymers. The conductive polymers were prepared by low cost, simple chemical synthesis methods and electrode fabrication via spin coating. We observe that the developed PASC device exhibited a specific capacitance of 13.22 $mF{\cdot}cm^{-2}$ with energy and power densities of 1.175 $\mu W{\cdot}h{\cdot}cm^{-2}$ and 4.99 $\mu W{\cdot}cm^{-2}$ at an applied current of 50 μA. As compared to the PTSC device (specific capacitance 3.30 $mF{\cdot}cm^{-2}$) the PASC shows four times higher specific capacitance due to its superior surface, structural and electrical properties. Further electrochemical impedance spectroscopic analysis (0.1 Hz to 100 kHz) shows that faster ionic exchange and high capacitance of the PASC electrode as compared to PTSC in H_3PO_4 electrolyte. We observed that the hydrophobicity is one of the key components in limiting the polythiophene performance, which can influence electrode and electrolyte interface. Also, the inferior surface, structural and electrical properties can limit its performance. We observed that as compared to polythiophene, PANI coating exhibits a uniform thin film which is found in the SEM image. The high resistance of the polythiophene electrode when reacting with solution reduces the energy-storing performances as observed in impedance analysis. The electrochemical performance reveals the enhanced SC performance for this preparation method of CP electrodes. For the pristine CP-based SCs, further studies are required for investigating various aqueous and gel electrolytes (acidic, alkaline, neutral, ionic liquids) influences on the electrochemical performances of the devices to fine-tune the best performances.

CRediT authorship contribution statement

Anjana Ramesh Peringath: Conceptualization, Methodology, Investigation, Writing- Original draft preparation, Validation: Mohammad A. H. Bayan: Conceptualization, Methodology, Investigation, Writing – original draft preparation; Mustehsan Beg: Investigation, Software; Amrita Jain: Investigation, Writing - reviewing and editing; Filippo Pierini: Investigation, Reviewing and Editing, Supervision; Nikolaj Gadegaard: Investigation, Reviewing and Editing, Supervision; Richard Hogg: Investigation, Reviewing and Editing, Supervision; Libu Manjakkal: Conceptualization, Methodology, Investigation, Writing- Original draft preparation, Reviewing and Editing, Supervision.

Declaration of competing interest

The authors declare that they have no known competing financial interests or personal relationships that could have appeared to influence the work reported in this paper.

Data availability

Data will be made available on request.

Acknowledgment

This work was supported by the NERC discipline hopping activities to tackle environmental challenges project (SEED-2022-317475). This work was partially supported by the National Science Centre (NCN) SONATA BIS Project No. 2020/38/E/ST5/00456. This work was also financially supported by the National Centre for Research and Development (NCBR, Poland); Project number: V4-Japan/2/17/AtomDeC/2022 under the Visegrad Group-Japan 2021 Joint Call on Advanced Materials in cooperation with the International Visegrad Fund. NG acknowledges funding from the Novo Nordisk Foundation Challenge Programme in Energy materials with biological applications (EMGUT): grant ref. No. NNF22OC0072961.

Appendix A. Supplementary data

Supplementary data to this article can be found online at https://doi.org/10.1016/j.est.2023.108811.

References

[1] Y. Liang, C.Z. Zhao, H. Yuan, Y. Chen, W. Zhang, J.Q. Huang, D. Yu, Y. Liu, M. M. Titirici, Y.L. Chueh, A review of rechargeable batteries for portable electronic devices, InfoMat 1 (1) (2019) 6–32.
[2] X. Xiao, Z. Zheng, X. Zhong, R. Gao, Z. Piao, M. Jiao, G. Zhou, Rational design of flexible Zn-based batteries for wearable electronic devices, ACS Nano 17 (3) (2023) 1764–1802.
[3] B. Huang, W. Zhang, J. Chen, Y. Cui, C. Zhu, S. Yan, Research Progress and prospects of Li-air battery in wearable devices, J. Electrochem. Soc. 170 (2023), 020506.
[4] L. Manjakkal, L. Yin, A. Nathan, J. Wang, R. Dahiya, Energy autonomous sweat-based wearable systems, Adv. Mater. 33 (35) (2021) 2100899.

[5] C. Xiong, T. Wang, Z. Zhao, Y. Ni, Recent progress in the development of smart supercapacitors, SmartMat 4 (2) (2023), e1158.
[6] M.S. Javed, T. Najam, I. Hussain, M. Idrees, A. Ahmad, M. Imran, S.S.A. Shah, R. Luque, W. Han, Fundamentals and scientific challenges in structural design of cathode materials for zinc-ion hybrid supercapacitors, Adv. Energy Mater. 13 (3) (2023) 2202303.
[7] X. Zhang, R. Han, Y. Liu, H. Li, W. Shi, X. Yan, X. Zhao, Y. Li, B. Liu, Porous and graphitic structure optimization of biomass-based carbon materials from 0D to 3D for supercapacitors: a review, Chem. Eng. J. 141607 (2023).
[8] L. Manjakkal, C.G. Núñez, W. Dang, R. Dahiya, Flexible self-charging supercapacitor based on graphene-Ag-3D graphene foam electrodes, Nano Energy 51 (2018) 604–612.
[9] L. Manjakkal, W.T. Navaraj, C.G. Núñez, R. Dahiya, Graphene–graphite polyurethane composite based high-energy density flexible supercapacitors, Adv. Sci. 6 (7) (2019) 1802251.
[10] D.B. Basha, S. Ahmed, A. Ahmed, M.A. Gondal, Recent advances on nitrogen doped porous carbon micro-supercapacitors: new directions for wearable electronics, J. Energy Storage 60 (2023), 106581.
[11] M. Al-Furjan, Z. Qi, L. Shan, A. Farrokhian, X. Shen, R. Kolahchi, Nano supercapacitors with practical application in aerospace technology: vibration and wave propagation analysis, Aerosp. Sci. Technol. 133 (2023), 108082.
[12] M.Y. Bhat, S. Hashmi, M. Khan, D. Choi, A. Qurashi, Frontiers and recent developments on supercapacitor's materials, design, and applications: transport and power system applications, J. Energy Storage 58 (2023), 106104.
[13] H.W. Park, K.C. Roh, Recent advances in and perspectives on pseudocapacitive materials for supercapacitors—a review, J. Power Source 557 (2023), 232558.
[14] M.M. Baig, I.H. Gul, S.M. Baig, F. Shahzad, 2D MXenes: synthesis, properties, and electrochemical energy storage for supercapacitors—a review, J. Electroanal. Chem. 904 (2022), 115920.
[15] R. Mendoza, J. Oliva, V. Rodriguez-Gonzalez, Effect of the micro-, meso-and macropores on the electrochemical performance of supercapacitors: a review, Int. J. Energy Res. 46 (6) (2022) 6989–7020.
[16] M.G. Say, C.J. Brett, J. Edberg, S.V. Roth, L.D. Söderberg, I. Engquist, M. Berggren, Scalable paper supercapacitors for printed wearable electronics, ACS Appl. Mater. Interface 14 (50) (2022) 55850–55863.
[17] S. Sardana, A. Gupta, K. Singh, A. Maan, A. Ohlan, Conducting polymer hydrogel based electrode materials for supercapacitor applications, J. Energy Storage 45 (2022), 103510.
[18] M.G. Sumdani, M.R. Islam, A.N.A. Yahaya, S.I. Safie, Recent advancements in synthesis, properties, and applications of conductive polymers for electrochemical energy storage devices: a review, Poly. Eng. Sci. 62 (2) (2022) 269–303.
[19] H. Jinno, T. Yokota, M. Koizumi, W. Yukita, M. Saito, I. Osaka, K. Fukuda, T. Someya, Self-powered ultraflexible photonic skin for continuous bio-signal detection via air-operation-stable polymer light-emitting diodes, Nat. Commun. 12 (2021) 1–9.
[20] A. Minotto, P.A. Haigh, Ł.G. Łukasiewicz, E. Lunedei, D.T. Gryko, I. Darwazeh, F. Cacialli, Visible light communication with efficient far-red/near-infrared polymer light-emitting diodes, Light Sci. Appl. 9 (1) (2020) 70.
[21] H. Zhou, Z. Wang, W. Zhao, X. Tong, X. Jin, X. Zhang, Y. Yu, H. Liu, Y. Ma, S. Li, W. Chen, Robust and sensitive pressure/strain sensors from solution processable composite hydrogels enhanced by hollow-structured conducting polymers, Chem. Eng. J. 403 (2021) 12307.
[22] L. Dan, A.L. Elias, Flexible and stretchable temperature sensors fabricated using solution-processable conductive polymer composites, Adv. Healthcare Mater. 9 (16) (2020) 2000380.
[23] Z. Xu, J. Song, B. Liu, S. Lv, F. Gao, X. Luo, P. Wang, A conducting polymer PEDOT: PSS hydrogel based wearable sensor for accurate uric acid detection in human sweat, Sensors Actuators B Chem. 348 (2021), 130674.
[24] S.V. Ebadi, H. Fashandi, D. Semnani, B. Rezaei, A. Fakhrali, Overcoming the potential drop in conducting polymer artificial muscles through metallization of electrospun nanofibers by electroplating process, Smart Mater. Struct. 29 (2020), 085036.
[25] S. Aziz, J.G. Martinez, J. Foroughi, G.M. Spinks, E.W.H. Jager, Artificial muscles from hybrid carbon nanotube-polypyrrole-coated twisted and coiled yarns, Macromol. Mater. Eng. 305 (11) (2020) 2000421.
[26] F. Hu, Y. Xue, J. Xu, B. Lu, PEDOT-based conducting polymer actuators, Front. Robot. AI 6 (2019) 114.
[27] S. Kanwal, Z. Akhter, N.Z. Ali, R. Hussainb, S. Qamar, Corrosion protection of aluminum alloy (AA2219-T6) using sulfonic acid-doped conducting polymer coatings, New J. Chem. 46 (2022) 14557–14564.
[28] M. Abd El-Ghaffar, N. Abdelwahab, A.M. Fekry, M. Sanad, M. Sabaa, S. Soliman, Polyester-epoxy resin/conducting polymer/barium sulfate hybrid composite as a smart eco-friendly anti-corrosive powder coating, Prog. Org. Coat. 144 (2020), 105664.
[29] L. Manjakkal, A. Pullanchiyodan, N. Yogeswaran, E.S. Hosseini, R. Dahiya, A wearable supercapacitor based on conductive PEDOT:PSS-coated cloth and a sweat electrolyte, Adv. Mater. 32 (24) (2020) 1907254.
[30] A.M. Bryan, L.M. Santino, Y. Lu, S. Acharya, J.M. D'Arcy, Conducting polymers for pseudocapacitive energy storage, Chem. Mater. 28 (17) (2016) 5989–5998.
[31] S. Narayanan, A.E. Pankajakshan, V.T. Padmanabhan, A. Joseph, Conducting polymer nanocomposites for supercapacitors, in: Polymer Nanocomposites in Supercapacitors, CRC Press, 2023, pp. 17–41.
[32] J. Stejskal, O.E. Bogomolova, N.V. Blinova, M. Trchová, I. Šeděnková, J. Prokeš, I. Sapurina, Mixed electron and proton conductivity of polyaniline films in aqueous solutions of acids: beyond the 1000 S cm^{-1} limit, Polym. Int. 58 (8) (2009) 872–879.
[33] Y. Huang, H. Li, Z. Wang, M. Zhu, Z. Pei, Q. Xue, Y. Huang, C. Zhi, Nanostructured polypyrrole as a flexible electrode material of supercapacitor, Nano Energy 22 (2016) 422–438.
[34] G.-F. Chen, Z.-Q. Liu, J.-M. Lin, N. Li, Y.-Z. Su, Hierarchical polypyrrole based composites for high performance asymmetric supercapacitors, J. Power Source 283 (2015) 484–493.
[35] C.I. Idumah, A review on polyaniline and graphene nanocomposites for supercapacitors, Polym. Plast. Technol. Mater. 61 (17) (2022) 1871–1907.
[36] M. Azimi, M. Abbaspour, A. Fazli, H. Setoodeh, B. Pourabbas, Investigation on electrochemical properties of polythiophene nanocomposite with graphite derivatives as supercapacitor material on breath figure-decorated PMMA electrode, J. Electron. Mater. 47 (3) (2018) 2093–2102.
[37] A.K. Thakur, M. Majumder, R.B. Choudhary, S.N. Pimpalkar, Supercapacitor based on electropolymerized polythiophene and multiwalled carbon nanotubes composites, IOP Conf. Ser. Mater. Sci. Eng. 149 (1) (2016), 012166.
[38] H. Gao, F. Wu, X. Wang, C. Hao, C. Ge, Preparation of $NiMoO_4$-PANI core-shell nanocomposite for the high-performance all-solid-state asymmetric supercapacitor, Int. J. Hydrog. Energy 43 (39) (2018) 18349–18362.
[39] D.S. Patil, J.S. Shaikh, S.A. Pawar, R.S. Devan, Y.R. Ma, A.V. Moholkar, J.H. Kim, R.S. Kalubarme, C.J. Park, P.S. Patil, Investigations on silver/polyaniline electrodes for electrochemical supercapacitors, Phys. Chem. Chem. Phys. 14 (34) (2012) 11886–11895.
[40] W.L. Liu, Y.Q. Guo, T. Lin, H.C. Peng, Y.P. Yu, F. Yang, S. Chen, High-performance supercapacitor electrodes of MXene/PANI/carbon fiber hybrid composites with 2D/0D/1D hierarchical nanostructures, J. Alloys Compd. 926 (2022), 166855.
[41] M.A.A. Mohd Abdah, N.H.N. Azman, S. Kulandaivalu, Y. Sulaiman, Review of the use of transition-metal-oxide and conducting polymer-based fibres for high-performance supercapacitors, Mater. Des. 186 (2020), 108199.
[42] T. Yuan, Z. Zhang, Q. Liu, X.-T. Liu, Y.-N. Miao, C.-L. Yao, MXene (Ti_3C_2Tx)/cellulose nanofiber/polyaniline film as a highly conductive and flexible electrode material for supercapacitors, Carbohydr. Polym. 304 (2023), 120519.
[43] P. Du, Y. Dong, H. Kang, J. Li, J. Niu, P. Liu, Superior cycle stability carbon layer encapsulated polyaniline nanowire core-shell nanoarray free-standing electrode for high performance flexible solid-state supercapacitors, J. Power Source 449 (2020), 227477.
[44] H. Vijith, S.P. Ashokkumar, L. Yesappa, M. Nirnjana, M. Vandana, H. Devaendrappa, Flexible and high energy density solid-state asymmetric supercapacitor based on polythiophene nanocomposites and charcoal, RASc Adv. (2018) 31414–31426.
[45] C. Bora, R. Pegu, B.J. Saikia, S.K. Dolui, Synthesis of polythiophene/graphene oxide composites by interfacial polymerization and evaluation of their electrical and electrochemical properties, Poly. Inter. 63 (12) (2014) 2061–2067.
[46] S. Zhao, Z. Song, L. Qing, J. Zhou, C. Qiao, Surface wettability effect on energy density and power density of supercapacitors, J. Phys. Chem. C 126 (22) (2022) 9248–9256.
[47] S. Lehtimaki, M. Suominen, P. Damlin, S. Tuukkanen, C. Kvarnstrom, D. Lupo, Preparation of supercapacitors on flexible substrates with electrodeposited PEDOT/graphene composites, ACS Appl. Mater. Interface 7 (40) (2015) 22137–22147.
[48] H. Habib, I.S. Wani, S. Husain, High performance nanostructured symmetric reduced graphene oxide/polyaniline supercapacitor electrode: effect of polyaniline morphology, J. Energy Storage 55 (2022), 105732.
[49] B. Song, L. Li, Z. Lin, Z.-K. Wu, K.-S. Moon, C.-P. Wong, Water-dispersible graphene/polyaniline composites for flexible micro-supercapacitors with high energy densities, Nano Energy 16 (2015) 470–478.
[50] J. Deng, T. Wang, J. Guo, P. Liu, Electrochemical capacity fading of polyaniline electrode in supercapacitor: an XPS analysis, Progr. Nat. Sci. Mater. Int. 27 (2) (2017) 257–260.
[51] J. Huang, Y. Xie, Y. You, J. Yuan, Q. Xu, H. Xie, Y. Chen, Rational design of electrode materials for advanced supercapacitors: from lab research to commercialization, Adv. Funct. Mater. 33 (14) (2023) 2213095.
[52] M. Yu, Y. Peng, X. Wang, F. Ran, Emerging design strategies toward developing next-generation implantable batteries and supercapacitors, Adv. Funct. Mater. 2301877 (2023).
[53] N. Gaikwad, P. Gadekar, B. Kandasubramanian, F. Kaka, Advanced polymer-based materials and mesoscale models to enhance the performance of multifunctional supercapacitors, J. Energy Storage 58 (2023), 106337.
[54] X. Chang, C.-W. Lin, A. Huang, M.F. El-Kady, R.B. Kaner, Molecular engineering of hierarchical conducting polymer composites for highly stable supercapacitors, Nano Lett. 23 (8) (2023) 3317–3325.